

A spatiotemporal analysis of the effect of ambient temperatures on the thermal behaviour of the Lunar Laser Ranging optical telescope at Hartebeesthoek Radio Astronomy Observatory

Philemon Tsela^{1,*}, Ludwig Combrinck^{2,1}, Bongani Ngcobo¹

¹Department of Geography, Geoinformatics and Meteorology, University of Pretoria, Pretoria, 0002, South Africa

²Space Geodesy Programme, Hartebeesthoek Radio Astronomy Observatory, P.O. Box 443, Krugersdorp, 1740 South Africa

*Corresponding author: philemon.tsela@up.ac.za

<http://dx.doi.org/10.4314/sajg.v5i3.8>

Abstract

Development of the 1-meter aperture Lunar Laser Ranging (LLR) telescope is underway at the Hartebeesthoek Radio Astronomy Observatory (HartRAO) which is expected to achieve sub-centimeter range precision and accuracy to the Moon, for enhanced tests of Earth-Moon system dynamics. Key to the operational performance of the telescope is thermal analysis of the telescope composite structure including the optical mirrors. This study presents a thermal analysis on the integrated component materials comprising the LLR telescope in ANSYS, with the aim of simulating its thermal behaviour in response to site-based ambient air temperature (T_A). Results show that for a full day T_A profile spanning the time period 00:00 to 23:59 the resulting range of simulated thermal variations measured at 12:00 midday and 23:59 nighttime across the telescope composite structure was found to be 9.11 °C to 10.03 °C and 9.12 °C to 9.86 °C respectively. In particular, the spider assembly and outer tube surface had the largest range of thermal variations i.e. greater than absolute 1 °C and thus, could be the main areas on the telescope where most thermal variations would occur. Furthermore, validation of the outer tube thermal variations using the 64 Resistant Temperature Detector (RTD) sensors mounted onto the test tube, showed reliable overall thermal variations of about 2 °C, at wind speeds of 0 to 0.4 km/h. In overall, these findings provide a typical expectation of the LLR telescope thermal behavior in response to T_A at the site; and thus could be used as a guide to develop an RTD-based thermal monitoring system for the HartRAO LLR optical telescope.

1. Introduction

Over the past 40 years, the occasional placement of retroreflectors on the lunar surface led to the evolution of the lunar laser ranging (LLR) technique. The placement was done by the manned APOLLO 11, 14 and 15 as well as the unmanned Soviet rover Lunakhod 1 and 2 missions (Bender *et al.*, 1973). These retroreflectors consists of reflective prism faces that return the incident laser beam to its original direction and as a result, provide the only means to measure the Earth-Moon distance with the LLR technique (Murphy, 2013). The LLR technique basically requires a telescope located at a ground station for transmitting a light pulse to a retroreflector on the Moon. After about 2.5 seconds the retroreflector returns the light pulse in the same direction; and therefore, the departure and arrival times of the light pulse are recorded at the station for deriving Earth-Moon distance measurements (Veillet *et al.*, 1993). Development of the new LLR geodetic station is underway at the Hartebeesthoek Radio Astronomy Observatory (HartRAO) of South Africa. This station is planned to acquire enhanced (millimetre) Earth-Moon distance measurements in the Southern Hemisphere (Munghemezulu *et al.*, 2016) using the refurbished ex-French 1-metre aperture telescope (Combrinck and Botha, 2013); and would be an addition to the five capable LLR stations based in the Northern Hemisphere (Noda *et al.*, 2014), namely the McDonald Observatory (Texas, U.S.A), Observatoire de la Côte d'Azur (France), Apache Point Observatory (New Mexico, U.S.A.), Matera (Italy) and Wettzell (Germany). Considering the uneven distribution of capable LLR stations worldwide, the HartRAO LLR station would play a significant role in the continuous global monitoring of the Earth-Moon system dynamics, as well as understanding the processes in the complex Earth system. According to Hofmann *et al.*, (2015), the current spatial distribution of LLR stations is likely to increase globally in the near future given the ongoing developmental efforts in other countries such as Russia (Vasilyev *et al.*, 2015), Japan (Noda *et al.*, 2014) and Chile (Fienga *et al.*, 2014).

The LLR measurements offer potentially more comprehensive solutions for accurate probes of the Moon's motion around the Earth, and the relative acceleration of both the Earth and Moon towards the Sun. This allows testing of the Einstein's Equivalence Principle, General Relativity Theory and the Time-rate-of-change in the gravitational constant G (Nordtvedt Jr, 1968; Williams *et al.*, 2009; Freire *et al.*, 2012). Some of the empirical findings based on analyses of long-term LLR measurements or geodetic observations to determine the dynamics of the Earth-Moon system include: (i) the annual Moon recession rate of about 3.8 cm away from the Earth (Murphy, 2013), and (ii) temporal changes in Newton's gravitational constant, G are constrained to $(2\pm 7)\times 10^{-13}$ per year which indicates the stableness of the universal force of gravity (Müller and Biskupek, 2007). These geodetic observations provide information that contributes to the derivation of global ranging data products which can be used in scientific activities spanning e.g. geophysics, oceanographic research, and geodesy for precise orbit determination and maintenance of the International Terrestrial Reference Frame (Combrinck, 2011).

One of the key factors in the operational performance of a ground-based optical laser telescope, particularly the LLR telescope, is thermal analysis of the telescope structure and

associated optics, based on the thermal properties of component materials and their interaction with the environment mainly through conventional heat transfer mechanisms (Bely, 2003, Greve and Bremer, 2010, Çengel and Ghajar, 2011). The relative effects induced by the heat transfer mechanisms e.g. conduction and convection, on the performance of the telescope vary both spatially and temporally (Bremer and Greve, 2011, Cho *et al.*, 2010, Vogiatzis *et al.*, 2014). In particular, thermal variations across the telescope due to variable ambient air temperatures (hereafter, denoted T_A) at the observatory site should be investigated in order to determine (i) the extent of their influence on the specified operational temperature range of critical components such as optics, detectors and supporting structure, (ii) their effect on achieving the pointing accuracy requirement of the telescope, and (iii) options for developing a thermal dynamic model for correcting the thermal variations.

Telescope thermal variations caused by T_A are usually analyzed using three widely known methods (Bely, 2003, Greve and Bremer, 2010). The first method entail simulating thermal variations using Finite element (FE) modelling software on a geometrically accurate three-dimensional model of the telescope, coupled with corresponding thermal loads of the component materials and typical spatio-temporal climatic parameters (Tsela *et al.*, 2015, Cho *et al.*, 2010, Ukita, 1999, Greve and MacLeod, 2011, Vogiatzis *et al.*, 2014). Furthermore, the reliability of thermal simulation results would depend to a large extent on the defined boundary conditions, correct parameterization of thermal loads which include e.g. T_A , film coefficient of air temperature (hereafter, denoted h) and material thermal properties (Cho *et al.*, 2010; Vogiatzis *et al.*, 2014). The second method is infrared thermography which uses a camera to detect photons of thermal infrared radiant energy exiting the target object, in the two primary thermal infrared (optimal atmospheric transmission) windows i.e. 3 - 5 μm and/or 8 -14 μm . The radiant energy is converted to temperature and thereafter an image of the object's (i.e. telescope's) temperature distribution is displayed (Jensen, 2009, Greve and Bremer, 2010, Yang and Chen, 2011). Lastly, the third method involves installation of several temperature sensors on strategically identified locations throughout the telescope's components. Thereafter, the acquired temperature measurements can be fed into a thermal dynamic model for timely monitoring, prediction and correction of the telescope's thermal variations (Tsela *et al.*, 2016, Pisanu *et al.*, 2010, Greve, and Kaercher, 2009, Murphy *et al.*, 2008, Greve *et al.*, 2005, Ukita, 1999). In this study, we opted for the first method in order to analyse thermal variations on the LLR optical telescope (Combrinck, 2011) based at HartRAO in South Africa.

In particular, several studies have used the first method described above for the analysis of thermal variations and related deformations, coupled with their consequent effect on the pointing performance of ground-based optical telescopes. For example, Cho *et al.* (2010) reported structural thermal variations due to varying T_A on the thirty meter telescope (TMT) ranging between 0.01 °C and 7.32 °C corresponding with thermally-induced deformations ranging between 141 μm and 993 μm respectively; and thus were shown to have a temporal impact on the telescope pointing with offsets ranging from 0.7" to 1" at selected elevation angles (Vogiatzis *et al.*, 2014). Mittag *et al.* (2008) analysed the influence of T_A on the pointing of the Hamburg robotic optical telescope for 16 nights (with temperatures ranging from -6.4°

C to 25.8° C) and found that thermal expansion of component materials primarily triggered misalignments of the optical axis with the tube. This expansion was responsible for the observed peak azimuth and elevation offsets of 40" and 10" respectively. Such studies indicate that the thermal behaviour of a site-based open-air optical telescope could impact on the required telescope performance (e.g. pointing) and, should therefore be investigated with respect to ambient climatic data, telescope's structural design and thermal properties of component materials.

The current study simulated the thermal behaviour of the integrated composite structure of the LLR optical telescope in ANSYS software (Lawrence, 2012) with respect to T_A typical of the HartRAO site. The simulations indicated varying magnitude of thermal variations expected for the telescope tube assembly and mount structure in its operating environment. In particular, thermally important areas which are likely to have large thermal variations across both the structural and optical components comprising the telescope were highlighted. While the impact of these findings is yet to be tested on the pointing performance of the LLR telescope (Combrinck, 2014); experimental results in other studies show that such thermal variations could influence (i) the link length between the primary and secondary mirrors, (ii) mirror curvature changes, and (iii) tube structural deformations (Atwood and O'Brien, 2003, Zheng *et al.*, 2012). Therefore, this study has significant implications for determining options for developing a thermal dynamic model that can mitigate and stringently regulate the overall thermal variations to ≤ 1 °C (Tsela *et al.*, 2016). These corrections would facilitate compensating for thermally-induced misalignment of the telescope axes, and potentially contribute toward the achievement of the required pointing accuracy of 0.5" (Combrinck, 2014).

2. System description

Various components of the LLR telescope are currently being integrated at HartRAO (Combrinck, 2011) coupled with the installation of modern instrumentation and development of sub-systems for operating the optical telescope (Tsela *et al.*, 2016, Munghezulu *et al.*, 2016, Combrinck and Botha, 2013). This telescope is a classical Cassegrain system (Figure 1) comprising various component materials such as Zerodur, Aluminium T6 7075 and Low carbon steel 1023 with varying thermal properties (Tsela *et al.*, 2015). These component materials are characteristic of (a) the concave 1-meter primary mirror and convex 0.3-meter secondary mirror, (b) baffle tube, inner and outer tube surfaces, and (c) primary mirror mount, fork assembly and outer ring support respectively (Figure 1).

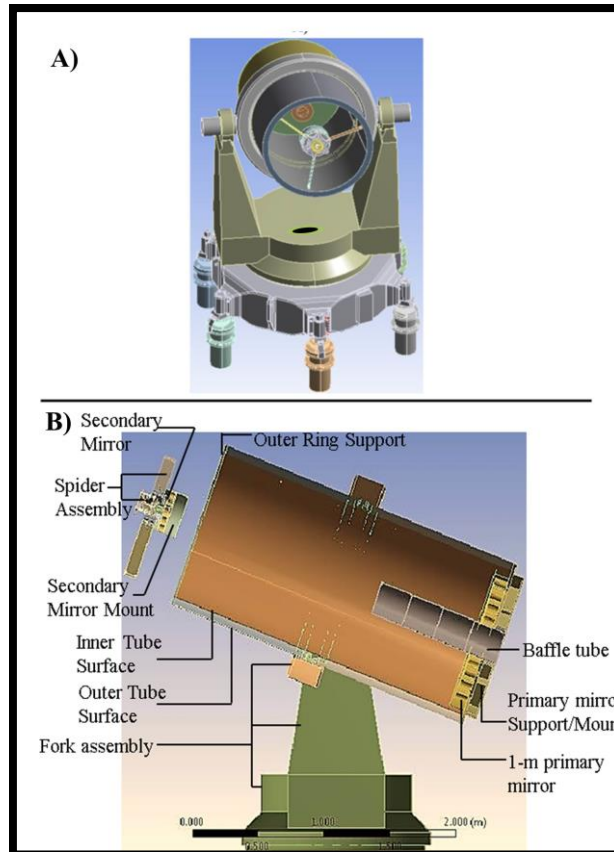


Figure 1: (A) A 3-dimensional model showing a complete view of the 1-m aperture optical telescope at the Hartebeesthoek Radio Astronomy Observatory, and (B) a side-view cross section of the telescope indicating the material components considered for thermal analysis in this study. The model (B) show the spider assembly in exploded view for legibility and does not include the telescope base i.e., pedestal and feet material components.

In principle, the outgoing/incoming laser light to/from the retro-reflectors mounted on the lunar surface will be transmitted/received through the primary mirror which is preferred for the sake of better laser light collimation (Combrinck, 2011). The telescope is expected to achieve pointing accuracy at 0.5 arcseconds level with estimated photons (detected at 532 nm wavelength) of 3-4 per minute based on the current 130 mJ, 80 pico-second pulse width system (Tsela *et al.*, 2015). Currently, a prototype pointing model operated on a 125 mm dual refractor testbed telescope (located in a fairly stable environment) achieved RMS error values at the 0.5 arcseconds level (Combrinck, 2014). It will be interesting to observe the extent of variation of the achieved values, particularly when the pointing model is tested on the actual LLR telescope which will be exposed to the varying thermal environment.

3. Methodology

3.1. Analysis of thermal variations

The analysis of thermal variations on the telescope composite structure (Figure 1 B) was performed in ANSYS software utilizing heat transfer equations [1] and [2]:

$$\vec{Q}_{cv} = hA_x(T_x - T_\infty)\hat{e}_x + hA_y(T_y - T_\infty)\hat{e}_y + hA_z(T_z - T_\infty)\hat{e}_z. \quad [1]$$

$$\vec{Q}_{cd} = -k(A_x \frac{\partial T}{\partial x} \hat{e}_x + A_y \frac{\partial T}{\partial y} \hat{e}_y + A_z \frac{\partial T}{\partial z} \hat{e}_z). \quad [2]$$

In Equation [1] \vec{Q}_{cv} represents the convection heat transfer rate between the telescope components and T_A at the HartRAO site. Here, h and T_∞ (synonymous with T_A) denote the film coefficient of air temperature ($W/m^2 \cdot ^\circ C$) and ambient air temperature ($^\circ C$) respectively; \hat{e}_x, \hat{e}_y and \hat{e}_z denotes the unit vectors; A_x, A_y and A_z represent the surface areas in meters; T_x, T_y and T_z are the temperatures in $^\circ C$ of the corresponding surfaces in three dimensional space of the assembled telescope structure respectively (Çengel, and Ghajar, 2011). Furthermore, in Equation [2] \vec{Q}_{cd} represent the conduction heat transfer rate through the telescope component materials as a result of their temperature difference ∂T in three dimensional space; and the thermal conductivity k in W/mK (Çengel, and Ghajar, 2011). Subsequent to the abovementioned heat transfer equations, the analysis of heat transfer by thermal radiation from the sun, sky and ground ought to be conducted particularly to understand the net radiation budget of the LLR telescope, and the overall effect on the telescope structure and operational performance. Such analysis is one of the important future considerations for the current study and will be reported in a separate paper.

The telescope composite structure (Figure 1 B) was assumed to be at an initial temperature of $9^\circ C$ and subsequently subjected to T_A typical of the HartRAO site encompassing a 24 hour time period for a particular day in June (winter). In this study, we assumed stationary air at room temperature around the telescope structure by adopting a constant h value of $0.025 W/m^2C$. This assumption thus excludes the wind effect during this thermal analysis. The wind effect including the varying h values representative of natural and/or forced convection are possible future considerations for the current analysis so as to approximate reality (as far as possible). The aforementioned ‘reality’, has so far only been analyzed with wind speeds of 0 to 0.4 km/h in this study, to analyze whether the wind has any significant changes to the telescope tube thermal variations. In overall, this analysis provided insight about the magnitude of thermal variations on and between the telescope components, particularly how these components thermally behaved in response to T_A .

3.2. Tube assembly experiments for the validation of derived thermal simulations

3.2.1. Tube structure and dimensions

The 1-meter aperture tube (Figure 2) which resembles the material and structural properties of the HartRAO LLR telescope tube (Tsela *et al.*, 2015) was used in this study, to conduct thermal experiments that were important for validating the derived thermal simulations.

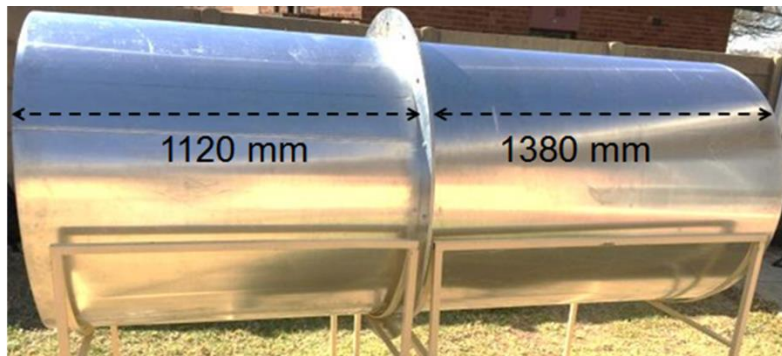


Figure 2. Aluminum tube structure used for conducting thermal experiments

The tube is a two-way separable structure with a combined length of about 2500 mm and a diameter of 1020 mm (Figure 2). Temperature sensors were mounted on the outer tube surface and arranged systematically (guided by the initial thermal simulation results reported in Tsela *et al.* (2015)) in order to measure the thermal variations across the entire tube surface.

3.2.2. Temperature sensors used

In this study, the F2020, 100 Ω , Class 'A' thin film resistant temperature detectors (RTDs) manufactured by OMEGA were selected in accordance with our thermal monitoring system's design specifications (HartRAO, 2005). The sensor's measurement accuracy levels are reportedly at ± 0.5 $^{\circ}\text{C}$ (or better given the observed ambient air temperature profiles of the HartRAO site (Tsela *et al.*, 2015)). Notwithstanding their utilization for thermal monitoring of one of the world's best LLR systems (Murphy *et al.*, 2008), RTDs have been widely reported to possess excellent accuracies over wide temperature range, improved linearization, long-term stability and an annual drift below 0.1°C (Greenhalgh *et al.*, 1994; Ibrahim, 2002, Sen *et al.*, 2011).

3.2.3. Calibration of sensors

The testing of accurate tube-temperature readings obtained by the mounted RTDs was conducted in this study. The DS18B20 1-wire digital thermometer was chosen for the testing, and has the accuracy of ± 0.5 $^{\circ}\text{C}$ for measured temperatures between -10 $^{\circ}\text{C}$ and $+85$ $^{\circ}\text{C}$. A total of 15 DS18B20 sensors were used and randomly mounted within the tube close to any of the 64 mounted RTDs (Figure 3).

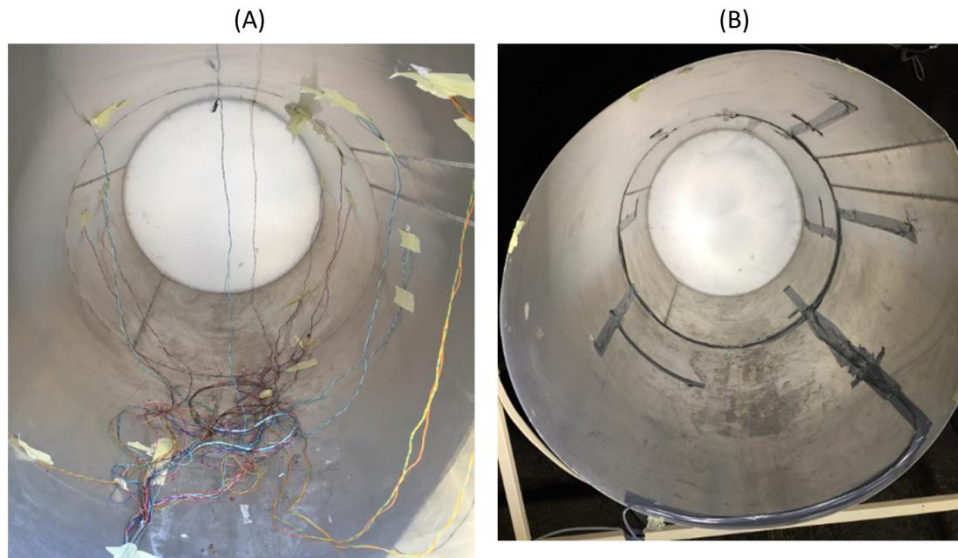


Figure 3. (A) Mounting of the 15 DS18B20 reference sensors within the tube. The back-end of the tube is fitted with polystyrene which represents an insulator, with virtually similar thermal properties to the 1-meter Zerodur primary mirror of the HartRAO LLR telescope. (B) Concealment of the 15 mounted DS18B20 reference sensors and wires within the tube using a grey insulation tape.

In particular, the DS18B20 sensors were used to calibrate and compare tube measurements obtained from the RTD sensors during day and night for successive days. The discrepancy between the RTD and DS18B20 concurrent temperature measurements at sampled locations on the tube was found to be on average ± 0.5 °C, and therefore both sensor types tend to be reading the same tube temperature.

3.2.4. Tube measurement setup

A total of 64 RTD sensors were systematically arranged and thermally bonded on the outer surface of the tube (Figure 4 and Figure 5). The illustration in Figure 4 was instrumental in the positioning, labeling and troubleshooting of RTD sensors. In particular, the arrangement of sensors on the tube is such that, they are equally spaced and dense as much as possible in order to determine a representative distribution of thermal variations of the tube structure relative to T_A .

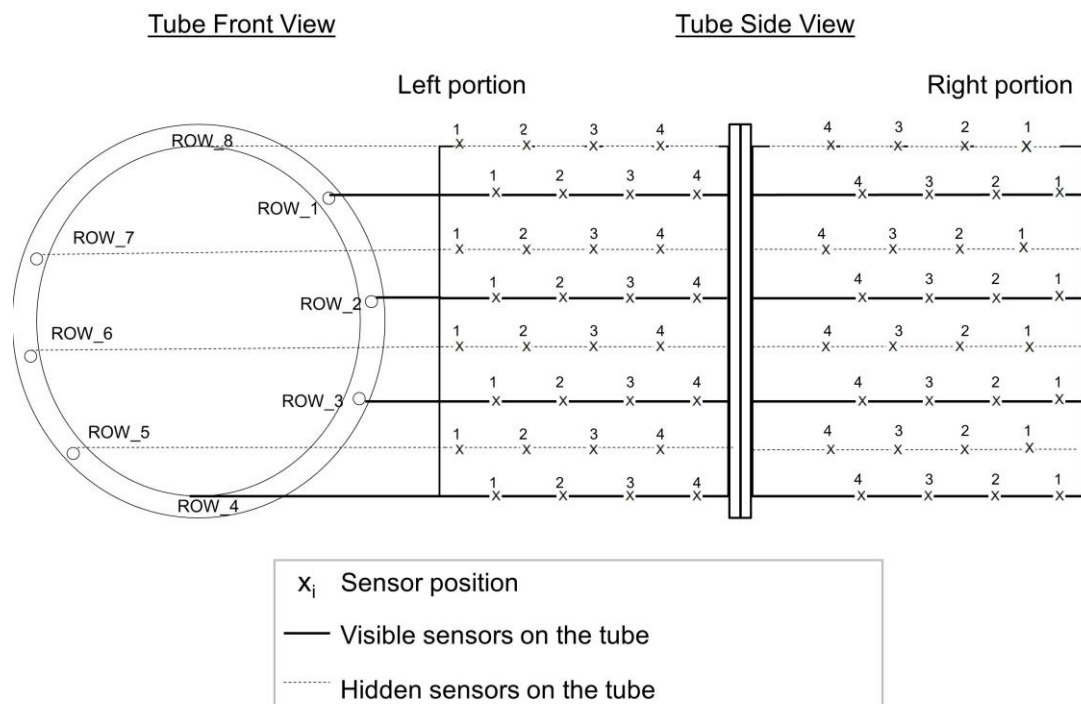


Figure 4. Placement of temperature sensors (RTDs) on the tube. The distance between sensors along the tube is approximately 140 mm whereas the distance between rows, around the tube is 127.5 mm.

The complete tube experiment setup comprising the tube, RTD sensors, digital multimeters as well as the wiring is shown in Figure 5. During the installation of RTD sensors it was necessary to verify and compare the temperature of particular RTD sensors. In particular, digital multimeters were used solely for this purpose. Fixed within the tube at specific, corresponding RTD sensor locations are the DS18B20 reference sensors. These reference sensors were used during the experiment as final calibration reference and to detect possible faulty sensors. The above procedure was necessary to ensure verified RTD sensor readings were acquired.



Figure 5. Troubleshooting and calibration setup of the tube showing the mounting and alignment of RTD sensors including the wiring and digital multimeters.

4. Results and discussion

4.1. Thermal analysis of the telescope

For T_A profile that varied from 9.1 °C to 23 °C at the site for a half day (00:00 – 12:00), the resulting minimum and maximum thermal variations measured at 12:00 midday across the telescope composite structure were in the range of 9.11 °C to 10.03 °C respectively (Figure 6). For a full day T_A profile spanning 00:00 – 23:59 the resulting range of thermal variations measured at 23:59 nighttime across the telescope composite structure was 9.12 °C to 9.86 °C (Figure 7). The discrepancy between the thermal variations depicted in multicolor isotherms on Figure 6 and Figure 7 indicate that the telescope experience more thermal variations (and related structural deformations (see Tsela *et al.* 2015)) during day time compared to nighttime. Further, it is evident that the thermal response time varies per component material primarily due to their respective thermal properties.

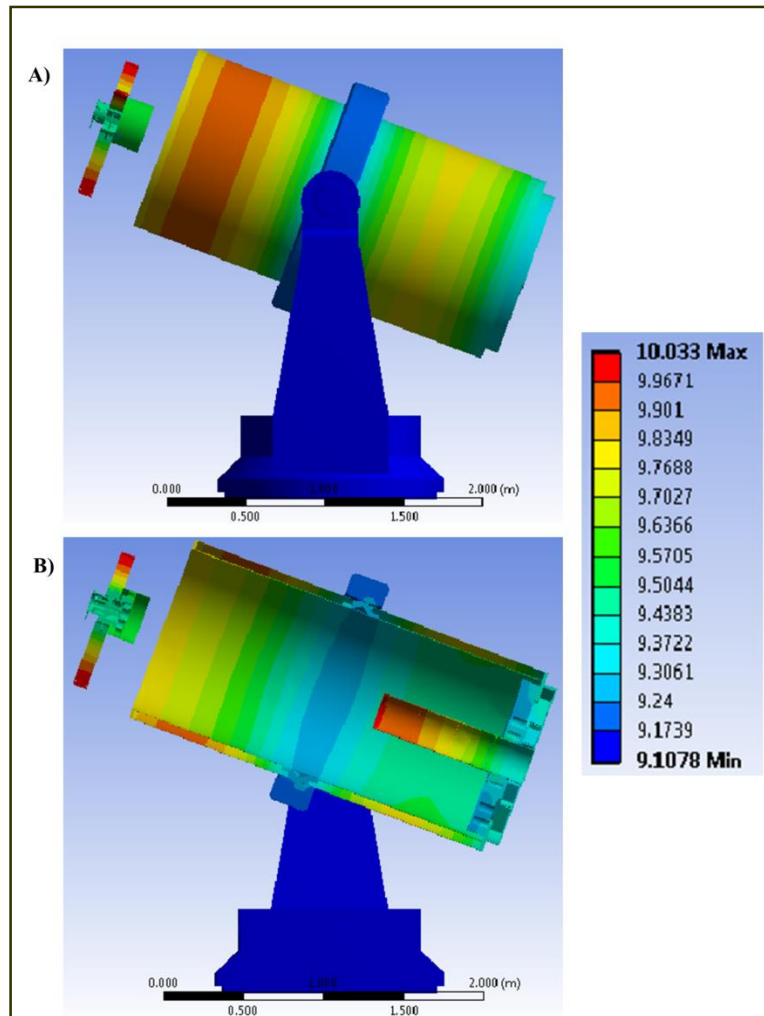


Figure 6. Full (A) and cross-section (B) of the telescope composite structure indicating the resulting thermal variations measured at 12:00 midday on the telescope components, in response to the T_A profile from the HartRAO site for the time period 00:00 – 12:00. The thermal variations ($^{\circ}\text{C}$) are represented by different coloured regions, each colour being an isotherm region; hence more colors correspond to more variations. Note the spider assembly in exploded view for legibility.

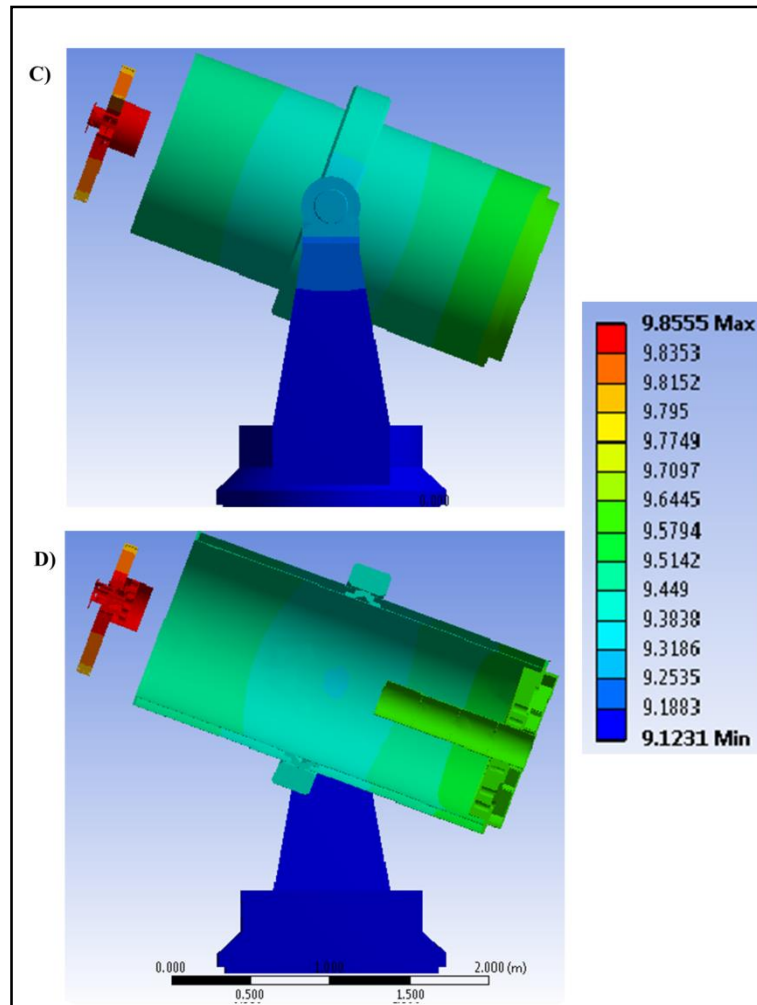


Figure 7. Full (C) and cross-section (D) of the telescope composite structure indicating the resulting thermal variations measured at 23:59 nighttime on the telescope components, in response to the T_A profile from the HartRAO site for the time period 00:00 – 23:59. The thermal variations ($^{\circ}\text{C}$) are represented by different coloured regions, each colour being an isotherm region; hence fewer colors correspond to fewer variations. Note the spider assembly in exploded view for legibility.

In particular, the spider assembly and outer tube surface had the largest range of thermal variations i.e. greater than absolute 1°C with corresponding high standard deviations (Table 1) and thus, could be the main areas on the telescope where most thermal variations are likely to occur. The primary mirror surface including its mount or support structure responds slowly to T_A with thermal variations of about 0.6°C (Table 1). In particular, these thermal variations had low variability (i.e. standard deviation) of 0.26°C and 0.24°C respectively (Table 1). Furthermore, the fork assembly (comprising the fork arms, elevation and azimuth mounts) had the smallest range of thermal variations (0.22°C) coupled with the lowest variability of 0.091°C (Table 1). The extent of thermal variations experienced by the telescope components including their thermal behavior given the full-day T_A profile of the HartRAO site is graphically shown in Figure 8.

Table 1. Descriptive statistics computed from the values of the telescope thermal state measured between 00:00 - 23:59. The sample size comprised of 145 recordings (°C) of the thermal state of the telescope composite structure taken at a sampling interval of 10 minutes within the time period of 00:00 – 23:59. The standard deviation indicates the variability of the 145 telescope thermal state values that were measured every 10 minutes throughout the day.

Model Input Variables	Range (max-min) of thermal variations °C	Average thermal variation °C	Standard deviation of thermal variations °C
Ambient Air	23.2-6.4 = 16.8	13.92	6.051
Telescope components			
Spider Assembly	10.29-9.042 = 1.248	9.680	0.445
Outer Tube Surface	10.14-9.076 = 1.064	9.587	0.374
Inner Tube Surface	10.06-9.073 = 0.987	9.537	0.356
Secondary Mirror Reflective Surface	9.874-9.037 = 0.837	9.497	0.346
Primary Mirror Reflective Surface	9.719-9.072 = 0.647	9.416	0.261
Primary Mirror Support/Mount	9.637-9.062 = 0.585	9.377	0.241
Ring Support	9.440-9.091 = 0.349	9.261	0.147
Fork Assembly	9.320-9.099 = 0.221	9.194	0.091

The sharp increase in T_A of the morning hours triggered the temperature change of all telescope components, which attempts to thermally respond to the T_A profile (Figure 8). Further, the continual rise of T_A particularly toward midday and early afternoon appears to trigger more thermal variations of the telescope components, with peak variations observed around 15:00 in the afternoon (Figure 8). During this time, we can expect the thermal state of the telescope composite structure not to be equipose, coupled with high thermal variations (of some components) exceeding 1 °C. While temperature of the telescope components collectively attempts to follow the decrease in T_A , it will be interesting to observe the time it takes for the telescope’s thermal state to reach internal equilibrium naturally, particularly post-midnight (Figure 8). In overall, the thermal variations depicted in Figures 6, 7 and 8 suggests the significance of forced-air ventilation procedures for temperature control, as these variations have been shown in other studies (Atwood and O'Brien, 2003, Zheng *et al.*, 2012, Tsela *et al.*, 2015) to induce structural displacements that could impact on the mirror reflective surface, link length between mirrors and consequent defocus of the lens. As a result, if such thermally-induced displacements are not properly accounted for, they could be detrimental to the required pointing accuracy of the HartRAO LLR optical telescope.

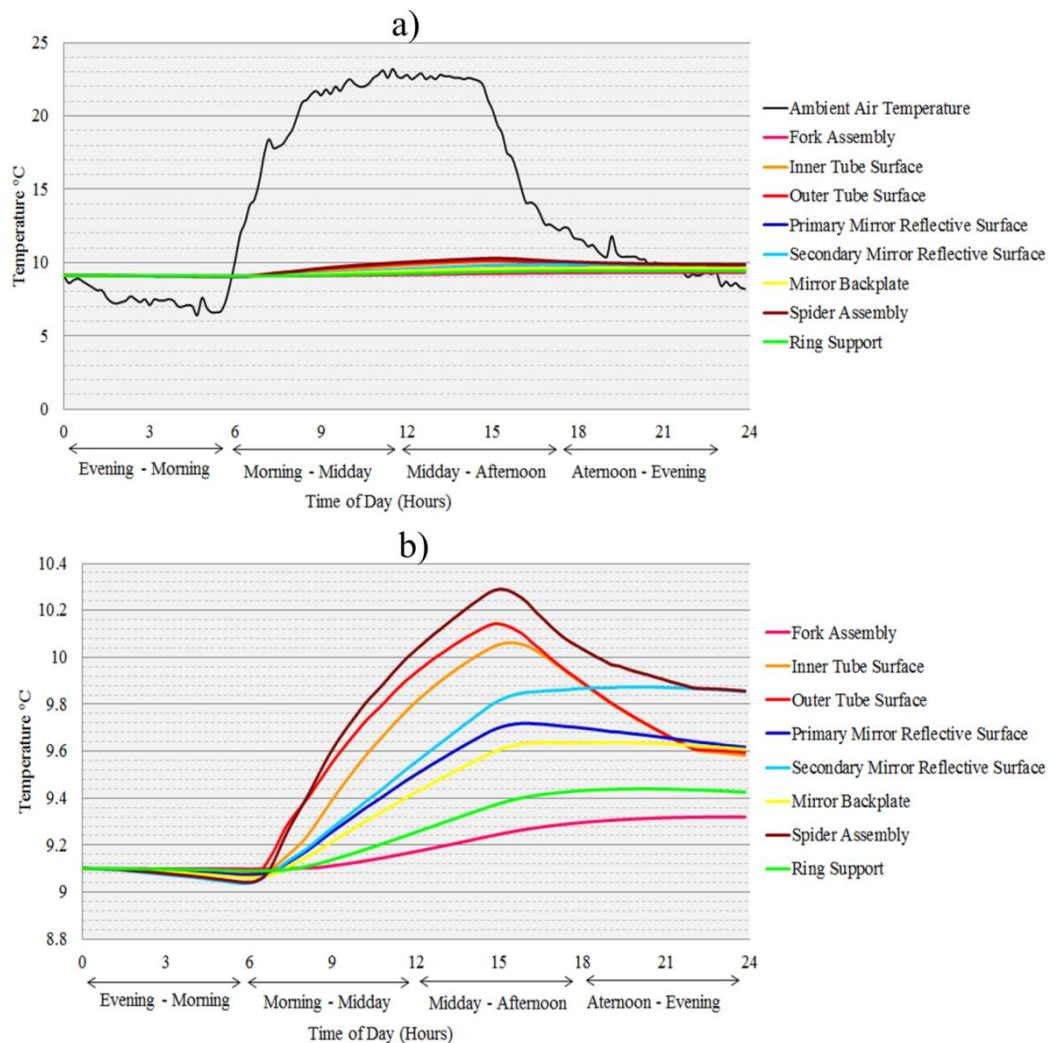


Figure 8. (a) Temperature changes measured at 10 minute intervals on the telescope component materials in relation to T_A typical of the HartRAO site during the time period 00:00 and 23:59 for a particular full-day in June. These temperature changes represent the thermal variations depicted in Figures 6 and 7 for the considered component materials; (b) Thermal variations in (a) shown in exploded view.

In particular, the corresponding range values of the secondary mirror indicate that it could be warmer than the primary mirror at end of day (Table 1; Figure 8). This outcome is partly due to the encapsulation of the secondary mirror within the spider assembly, and more importantly, the mechanical composition of the spider assembly (particularly at the centre where the mirror is mounted) appears to be manufactured in a manner that traps heat according to our thermal simulations (Figure 7). On the other hand, the primary mirror's range values (Table 1) indicate that, toward end of day i.e. 23:59 when T_A has dropped, the primary mirror would be warmer than any of its contacting surfaces (Figure 7, Figure 8). The apparent thermal variations of the mirrors are consistent with the thermal properties of the Zerodur mirror, especially their low k and coefficient of thermal expansion (CTE) values (Jedamzik *et al.*, 2010). However, timely equalization of these thermal variations on the mirrors including their respective contacting

surfaces, is important for overall optical and pointing performance of the telescope (Perry, 1943, Mittag *et al.*, 2008).

4.2. Validation of thermal simulations

Results of temperature measurements acquired using the 64 RTD sensors mounted onto the outer tube surface, reveal tube overall thermal variations of about 2 °C (Figure 9). For illustration purposes, the sample of measurements were taken in the morning hours of 5th May 2016 (winter season) i.e., for the time period of 05:25 - 05:55 am and 06:45 - 07:15 am in a fairly stable environment marked by recorded wind speed of about 0 km/h and 0.4 km/h respectively. The results of the tube experiment showed that at wind speeds of 0 and 0.4km/h there was no significant change on the telescope (tube) thermal variations (Figure 9). Further, during the night or early morning hours prior to sunrise, the tube surface temperature generally tends to be constant, with virtually no bulk temperature fluctuations along the tube surface detected by the RTD sensors (Figure 9 (a)).

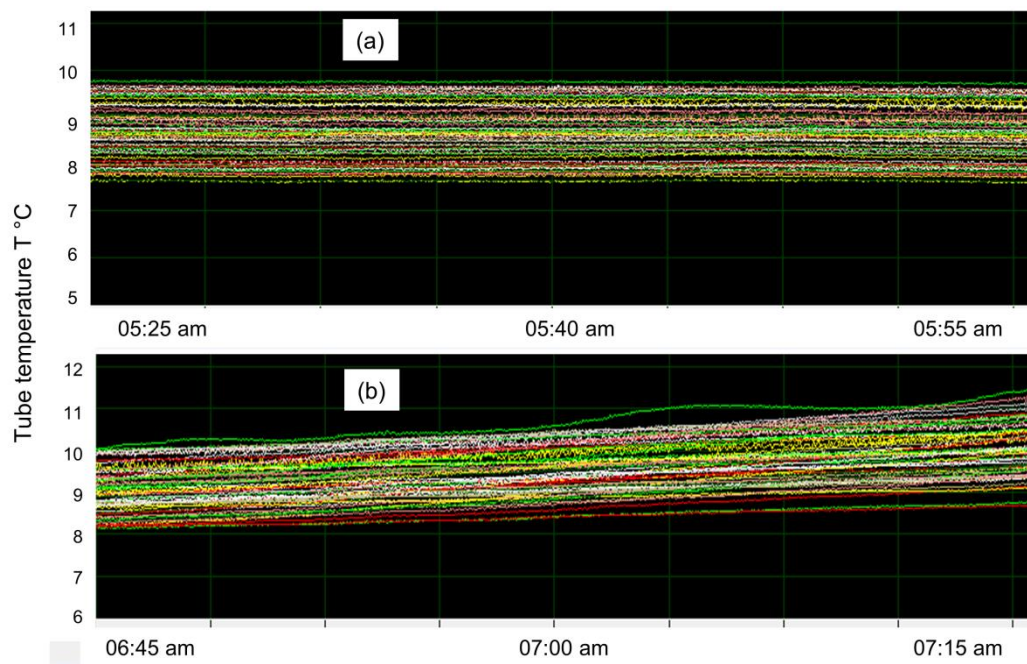


Figure 9. Recorded temperature (°C) versus time (hours) of 64 RTD sensors at two wind speeds, (a) 0 km/h and (b) 0.4 km/h. The wind was flowing parallel to the tube axis at the times of recording the RTD tube temperature measurements.

A subsequent gradual rise of thermal variations can be observed and represent the tube's thermal response to the fluctuations in T_A (Figure 9 (b)). Additionally, this gradual rise is due to the tube's horizontal position (Figure 5) which mainly exposes the upper arc of the tube surface to incoming solar radiation. Notably, the acquired tube-sensor temperature readings do not entirely overlap with each other and thus, the little gaps in between, could be an indication that the temperature along tube structure is not entirely the same (Figure 9). For example, this

assertion can be corroborated by the simulation results which showed varying temperatures between the middle and front-end of the tube (see Figure 6 and Figure 7). In addition, the observed thermal behavior of the tube from the experiment (Figure 9) show similar trends with the thermal simulation profile of the outer tube surface at corresponding times (Figure 8 (b)). Overall, the individual tube-sensor readings have a thermal variation of approximately 2 °C coupled with an error of ± 0.5 °C associated with each RTD sensor.

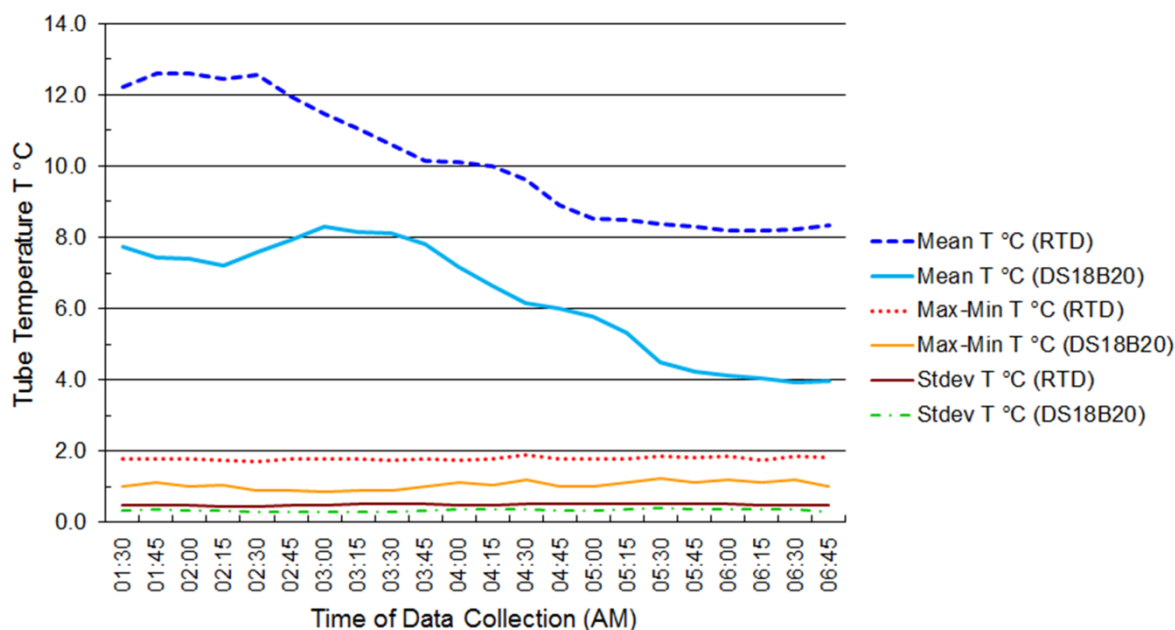


Figure 10. Comparison between DS18B20 and RTD temperature measurements that were simultaneously acquired at 15 corresponding locations on the tube for the time period 01:30 – 06:45 am on 5th May 2016.

The differences between the minimum and the maximum temperature, from the 15 sensors of the DS18B20 and RTD at a sampling rate of 1 second for every 15 minutes over the time period of 01:30 am to 06:45 am were 1.04 °C and 1.79 °C respectively (Figure 10). Additionally, the standard deviations for the tube temperature by the aforementioned sensors were 0.04 °C and 0.02 °C respectively. During the night or time period considered, the tube temperature resembles an isotherm coupled with minor variations of the tube temperature sensor readings. On average, there is a notable trend agreement of a decline in tube temperature measured by both sensors simultaneously over the time period considered (Figure 10). Overall, these findings indicate that the RTD sensors used, have the potential to acquire accurate measurements and representative thermal variations of the telescope tube structure, and can be further tested on other components of the LLR telescope.

5. Conclusion

Development of the new LLR geodetic station is underway at the HartRAO of South Africa, and is expected to acquire enhanced (millimetre) Earth-Moon distance measurements through

the 1-meter aperture LLR telescope. Key to the successful achievement of millimetric Earth-Moon distance measurements is thermal analysis of the telescope composite structure including the optical mirrors, with respect to the varying ambient air temperatures at the site. This study presented a thermal analysis on integrated component materials comprising the telescope, with the aim of simulating its thermal behaviour in relation to site-based ambient air temperature. Results show that for a full day T_A profile spanning the time period 00:00 to 23:59 the resulting range of simulated thermal variations measured at 12:00 midday and 23:59 nighttime across the telescope composite structure was found to be 9.11 °C to 10.03 °C and 9.12 °C to 9.86 °C respectively. In particular, the spider assembly and outer tube surface had the largest range of thermal variations i.e. greater than absolute 1 °C and thus, could be the main areas on the telescope where most thermal variations would occur. Furthermore, validation of the outer tube thermal variations using the 64 Resistant Temperature Detector (RTD) sensors mounted onto the test tube, showed reliable overall thermal variations of about 2 °C, at wind speeds of 0 to 0.4 km/h. These findings have significant implications for (i) understanding the thermal behavior of the telescope, (ii) guiding the optimal location of sensors across thermally important areas of the telescope, and (iii) exploring options for developing a thermal dynamic model which would monitor and correct for thermal variations and subsequently feed these corrections into a telescope pointing model, to counteract resulting thermally-induced pointing offsets. In particular, thermal regulatory measures may be necessary to ensure these variations are equalized to $\leq 1^\circ \text{C}$ (Tsela *et al.*, 2016) which could contribute toward increasing the chance of being on-target with the retroreflectors located on the lunar surface. Additionally, gravity and wind are additional factors that require development of analytical models to investigate their induced relative effects on the pointing performance of the LLR optical telescope. The models, particularly on gravity-induced deformations of the telescope primary mirror are being studied in collaboration with other research teams at HartRAO (Nkosi *et al.*, 2016).

Acknowledgement

Philemon Tsela hereby acknowledges research support in part by the National Research Foundation of South Africa for the grant, Unique Grant No. 93952. Any opinion, finding and conclusion or recommendation expressed in this material is that of the author(s) and the NRF does not accept any liability in this regard. Further, the authors express their gratitude to the Inkaba yeAfrica project, the Department of Science and Technology of South Africa and HartRAO for support.

References

- Atwood, B. and O'Brien, T.P., 2003, March. Adjustable truss for support, optical alignment, and athermalization of a Schmidt camera. In *Astronomical Telescopes and Instrumentation* (pp. 403-410). International Society for Optics and Photonics.
- Bely, P. ed., 2003. *The design and construction of large optical telescopes*. Springer Science and Business Media.

- Bender, P.L., Currie, D.G., Poultney, S.K., Alley, C.O., Dicke, R.H., Wilkinson, D.T., Eckhardt, D.H., Faller, J.E., Kaula, W.M., Mulholland, J.D. and Plotkin, H.H., 1973. The lunar laser ranging experiment. *Science*, 182(4109), pp.229-238.
- Bremer, M. and Greve, A., 2011, September. A dynamic thermal model for design and control of an 800-element open-air radio telescope. In *Integrated Modeling of Complex Optomechanical Systems* (pp. 83360U-83360U). International Society for Optics and Photonics.
- Baars, J.W.M., Hooghoudt, B.G., Greve, A. and Penalver, J., 1988. Thermal control of the IRAM 30-m millimeter radio telescope. *Astronomy and Astrophysics*, 195, pp.364-371.
- Çengel, Y. A., and Ghajar, A. J. 2011. Heat and mass transfer: fundamentals and applications: McGraw-Hill.
- Cho, M., Corredor, A., Vogiatzis, K. and Angeli, G., 2010, July. Thermal analysis of the TMT telescope structure. In *SPIE Astronomical Telescopes+ Instrumentation* (pp. 77380C-77380C). International Society for Optics and Photonics.
- Combrinck, L., 2011, October. Development of a satellite and lunar laser ranger and its future applications in South Africa. In *Proceedings of the 62nd international astronomical congress*.
- Combrinck, L. 2014. Development of a high accuracy, user-friendly Lunar Laser Ranging telescope steering and pointing software package at HartRAO. Presented at the 19th International Workshop on Laser Ranging, Annapolis, Maryland.
- Combrinck, L., and Botha, R., 2013. Challenges and progress with the development of a lunar laser ranger for South Africa. Presented at the 18th International Workshop on Laser Ranging, Fujiyoshida, Japan.
- Fienga, A., Courde, C., Torre, J.M., Manche, H., Murphy, T., Mueller, J., Laskar, J., Bouquillon, S., Biskupek, L., Hofmann, F. and Capitaine, N., 2014. Interests of a new lunar laser instrumentation on the ESO NTT Telescope. *arXiv preprint arXiv:1405.0473*.
- Freire, P.C., Wex, N., Esposito-Farèse, G., Verbiest, J.P., Bailes, M., Jacoby, B.A., Kramer, M., Stairs, I.H., Antoniadis, J. and Janssen, G.H., 2012. The relativistic pulsar–white dwarf binary PSR J1738+0333–II. The most stringent test of scalar–tensor gravity. *Monthly Notices of the Royal Astronomical Society*, 423(4), pp.3328-3343.
- Greve, A. and Bremer, M., 2010. *Thermal design and thermal behaviour of radio telescopes and their enclosures* (Vol. 364). Springer Science & Business Media.
- Greve, A., Bremer, M., Penalver, J., Raffin, P. and Morris, D., 2005. Improvement of the IRAM 30-m telescope from temperature measurements and finite-element calculations. *Antennas and Propagation, IEEE Transactions on*, 53(2), pp.851-860.
- Greve, A. and MacLeod, G., 2001. Thermal model calculations of enclosures for millimeter wavelength radio telescopes. *Radio Science*, 36(5), pp.1111-1128.
- Greve, A. and Kaercher, H.J., 2009. Performance improvement of a flexible telescope through metrology and active control. *Proceedings of the IEEE*, 97(8), pp.1412-1420.
- Greenhalgh, R.J.S., Stepp, L.M. and Hansen, E.R., 1994, June. Gemini primary mirror thermal management system. In *1994 Symposium on Astronomical Telescopes & Instrumentation for the 21st Century* (pp. 911-921). International Society for Optics and Photonics.

- Hofmann, F., Müller, J. Biskupek, L. 2015. Lunar Laser Ranging: Das Erde-Mond-System und Tests der Einstein'schen Gravitationstheorie, *zfv*, Jg. 140, S. 337-345, DOI: 10.12902/zfv-0087-2015.
- Ibrahim, D., 2002. Microcontroller-based temperature monitoring and control. Newnes, Oxford, United Kingdom, 236pp. Ibrahim, D., 2002. *Microcontroller-based temperature monitoring and control*. Newnes.
- Hartebeesthoek Radio Astronomy Observatory (HartRAO). 2005. Proposed re-location and conversion of CNES SLR system to South Africa in collaboration with OCA and the greater ILRS community. Retrieved August, 2013, from http://www.hartrao.ac.za/iisgeo/docs/LLR_proposal.doc.
- Jensen, J.R., 2009. *Remote sensing of the environment: An earth resource perspective 2/e*. Pearson Education India.
- Mittag, M., Hempelmann, A., Gonzalez-Perez, J.N. and Schmitt, J.H.M.M., 2008. The temperature dependence of the pointing model of the hamburg robotic telescope. *Publications of the Astronomical Society of the Pacific*, 120(866), p.425.
- Müller, J. and Biskupek, L., 2007. Variations of the gravitational constant from lunar laser ranging data. *Classical and Quantum Gravity*, 24(17), p.4533.
- Murphy Jr, T.W., Adelberger, E.G., Battat, J.B.R., Carey, L.N., Hoyle, C.D., LeBlanc, P., Michelsen, E.L., Nordtvedt, K., Orin, A.E., Strasburg, J.D. and Stubbs, C.W., 2008. The apache point observatory lunar laser-ranging operation: instrument description and first detections. *Publications of the Astronomical Society of the Pacific*, 120(863), p.20.
- Murphy, T.W., 2013. Lunar laser ranging: the millimeter challenge. *Reports on Progress in Physics*, 76(7), p.076901.
- Munghemezulu, C., Combrinck, L. and Botai, J.O., 2016. A review of the lunar laser ranging technique and contribution of timing systems. *South African Journal of Science*, 112(3-4), pp.1-9.
- Noda, H., Kunimori, H. and Araki, H., 2014, March. Lunar Laser Ranging Experiment at Koganei SLR Station. In *Lunar and Planetary Science Conference* (Vol. 45, p. 1638).
- Nordtvedt Jr, K., 1968. Equivalence principle for massive bodies. II. Theory. *Physical Review*, 169(5), p.1017.
- Nkosi, N., Combrinck, W.L. and Akombelwa, M., 2016. Optical configuration and optical tests of the HartRAO Lunar Laser Ranger. *South African Journal of Geology*, 119(1), pp.99-108.
- Perry, J.W., 1943. Thermal effects upon the performance of lens systems. *Proceedings of the Physical Society*, 55(4), p.257.
- Pisanu, T., Buffa, F., Morsiani, M., Pernechele, C. and Poppi, S., 2010, July. Thermal behavior of the Medicina 32-meter radio telescope. In *SPIE Astronomical Telescopes+ Instrumentation* (pp. 773935-773935). International Society for Optics and Photonics.
- Sen, S.K., Pan, T.K. and Ghosal, P., 2011. An improved lead wire compensation technique for conventional four wire resistance temperature detectors (RTDs). *Measurement*, 44(5), pp.842-846.
- Tsela, P., Combrinck, L., Botha, R. and Ngcobo, B., 2015. Thermal analysis of the LLR optical telescope tube assembly based in Hartebeesthoek Radio Astronomy Observatory. *Acta Geodaetica et Geophysica*, pp.1-11.

- Tsela, P., Combrinck, L., Botha, R., and Ngcobo, B. 2016. A proposed mathematical model of thermal variations on the HartRAO Lunar Laser Ranging telescope for enhanced tests of Earth-Moon system dynamics. *South African journal of Geology*, 119(1): 83-90.
- Ukita, N., 1999. Thermal effects on the pointing of the Nobeyama 45-m telescope. Publications of the National Astronomical Observatory of Japan, 5, pp.139-147.
- Vasilyev, M.V., Yagudina, E.I., Torre, J.M. and Feraudy, D., 2015, August. Planned LLR station in Russia and its impact on the Lunar Ephemeris Accuracy. In *Proceedings of the Journées 2014* (Vol. 1, p. 112).
- Veillet, C., Mangin, J.F., Chabaudie, J.E., Dumolin, C., Feraudy, D. and Torre, J.M., 1993. Lunar Laser Ranging at CERGA for the Ruby Period (1981-1986). *Contributions of Space Geodesy to Geodynamics: Technology*, pp.189-193.
- Vogiatzis, K., Sadjadpour, A. and Roberts, S., 2014, August. TMT telescope structure thermal model. In *SPIE Astronomical Telescopes+ Instrumentation* (pp. 915011-915011). International Society for Optics and Photonics.
- Williams, J.G., Turyshv, S.G. and Boggs, D.H., 2009. Lunar laser ranging tests of the equivalence principle with the earth and moon. *International Journal of Modern Physics D*, 18(07), pp.1129-1175.
- Williams, J. G. and Dickey, J. O. 2002. Lunar Geophysics, Geodesy and Geodynamics. Proceedings of the 13th International Workshop on Laser Ranging, Washington, D.C., United States of America, 7-11 October 2002, 75-86.
- Yang, R. and Chen, Y., 2011. Design of a 3-D infrared imaging system using structured light. *Instrumentation and Measurement, IEEE Transactions on*, 60(2), pp.608-617.